Measurement of the spectral function for the $\tau^- \to K^- K_S \nu_\tau$ decay

J. P. Lees,[1] V. Poireau,[1] V. Tisserand,[1] E. Grauges,[2] A. Palano,[3] G. Eigen,[4] D. N. Brown,[5] Yu. G. Kolomensky,[5] M. Fritsch,[6] H. Koch,[6] T. Schroeder,[6] C. Hearty,[7a,7b] T. S. Mattison,[7b] J. A. McKenna,[7b] R. Y. So,[7b] V. E. Blinov,[8a,8b,8c] A. R. Buzykaev,[8a] V. P. Druzhinin,[8a,8b] V. B. Golubev,[8a,8b] E. A. Kozyrev,[8a,8b] E. A. Kravchenko,[8a,8b] A. P. Onuchin,[8a,8b,8c] S. I. Serednyakov,[8a,8b] Yu. I. Skovpen,[8a,8b] E. P. Solodov,[8a,8b] K. Yu. Todyshev,[8a,8b] A. J. Lankford,[9] J. W. Gary,[10] O. Long,[10] A. M. Eisner,[11] W. S. Lockman,[11] W. Panduro Vazquez,[11] D. S. Chao,[12] C. H. Cheng,[12] B. Echenard,[12] K. T. Flood,[12] D. G. Hitlin,[12] J. Kim,[12] Y. Li,[12] T. S. Miyashita,[12] P. Ongmongkolkul,[12] F. C. Porter,[12] M. Röhrken,[12] Z. Huard,[13] B. T. Meadows,[13] B. G. Pushpawela,[13] M. D. Sokoloff,[13] L. Sun,[13,*] J. G. Smith,[14] S. R. Wagner,[14] D. Bernard,[15] M. Verderi,[15] D. Bettoni,[16a] C. Bozzi,[16a] R. Calabrese,[16a,16b] G. Cibinetto,[16a,16b] E. Fioravanti,[16a,16b] I. Garzia,[16a,16b] E. Luppi,[16a,16b] V. Santoro,[16a] A. Calcaterra,[17] R. de Sangro,[17] G. Finocchiaro,[17] S. Martellotti,[17] P. Patteri,[17] I. M. Peruzzi,[17] M. Piccolo,[17] M. Rotondo,[17] A. Zallo,[17] S. Passaggio,[18] C. Patrignani,[18,†] H. M. Lacker,[19] B. Bhuyan,[20] U. Mallik,[21] C. Chen,[22] J. Cochran,[22] S. Prell,[22] A. V. Gritsan,[23] N. Arnaud,[24] M. Davier,[24] F. Le Diberder,[24] A. M. Lutz,[24] G. Wormser,[24] D. J. Lange,[25] D. M. Wright,[25] J. P. Coleman,[26] E. Gabathuler,[26,‡] D. E. Hutchcroft,[26] D. J. Payne,[26] C. Touramanis,[26] A. J. Bevan,[27] F. Di Lodovico,[27] R. Sacco,[27] G. Cowan,[28] Sw. Banerjee,[29] D. N. Brown,[29] C. L. Davis,[29] A. G. Denig,[30] W. Gradl,[30] K. Griessinger,[30] A. Hafner,[30] K. R. Schubert,[30] R. J. Barlow,[31,§] G. D. Lafferty,[31] R. Cenci,[32] A. Jawahery,[32] D. A. Roberts,[32] R. Cowan,[33] S. H. Robertson,[34a,34b] R. M. Seddon,[34b] B. Dey,[35a] N. Neri,[35a] F. Palombo,[35a,35b] R. Cheaib,[36] L. Cremaldi,[36] R. Godang,[36,¶] D. J. Summers,[36] P. Taras,[37] G. De Nardo,[38] C. Sciacca,[38] G. Raven,[39] C. P. Jessop,[40] J. M. LoSecco,[40] K. Honscheid,[41] R. Kass,[41] A. Gaz,[42a] M. Margoni,[42a,42b] M. Posocco,[42a] G. Simi,[42a,42b] F. Simonetto,[42a,42b] R. Stroili,[42a,42b] S. Akar,[43] E. Ben-Haim,[43] M. Bomben,[43] G. R. Bonneaud,[43] G. Calderini,[43] J. Chauveau,[43] G. Marchiori,[43] J. Ocariz,[43] M. Biasini,[44a,44b] E. Manoni,[44a] A. Rossi,[44a] G. Batignani,[45a,45b] S. Bettarini,[45a,45b] M. Carpinelli,[45a,45b,**] G. Casarosa,[45a,45b] M. Chrzaszcz,[45a] F. Forti,[45a,45b] M. A. Giorgi,[45a,45b] A. Lusiani,[45a,45c] B. Oberhof,[45a,45b] E. Paoloni,[45a,45b] M. Rama,[45a] G. Rizzo,[45a,45b] J. J. Walsh,[45a] L. Zani,[45a,45b] A. J. S. Smith,[46] F. Anulli,[47a] R. Faccini,[47a,47b] F. Ferrarotto,[47a] F. Ferroni,[47a,47b] A. Pilloni,[47a,47b] G. Piredda,[47a,‡] C. Bünger,[48] S. Dittrich,[48] O. Grünberg,[48] M. Heß,[48] T. Leddig,[48] C. Voß,[48] R. Waldi,[48] T. Adye,[49] F. F. Wilson,[49] S. Emery,[50] G. Vasseur,[50] D. Aston,[51] C. Cartaro,[51] M. R. Convery,[51] J. Dorfan,[51] W. Dunwoodie,[51] M. Ebert,[51] R. C. Field,[51] B. G. Fulsom,[51] M. T. Graham,[51] C. Hast,[51] W. R. Innes,[51,‡] P. Kim,[51] D. W. G. S. Leith,[51] S. Luitz,[51] D. B. MacFarlane,[51] D. R. Muller,[51] H. Neal,[51] B. N. Ratcliff,[51] A. Roodman,[51] M. K. Sullivan,[51] J. Va'vra,[51] W. J. Wisniewski,[51] M. V. Purohit,[52] J. R. Wilson,[52] A. Randle-Conde,[53] S. J. Sekula,[53] H. Ahmed,[54] M. Bellis,[55] P. R. Burchat,[55] E. M. T. Puccio,[55] M. S. Alam,[56] J. A. Ernst,[56] R. Gorodeisky,[57] N. Guttman,[57] D. R. Peimer,[57] A. Soffer,[57] S. M. Spanier,[58] J. L. Ritchie,[59] R. F. Schwitters,[59] J. M. Izen,[60] X. C. Lou,[60] F. Bianchi,[61a,61b] F. De Mori,[61a,61b] A. Filippi,[61a] D. Gamba,[61a,61b] L. Lanceri,[62] L. Vitale,[62] F. Martinez-Vidal,[63] A. Oyanguren,[63] J. Albert,[64b] A. Beaulieu,[64b] F. U. Bernlochner,[64b] G. J. King,[64b] R. Kowalewski,[64b] T. Lueck,[64b] I. M. Nugent,[64b] J. M. Roney,[64b] R. J. Sobie,[64a,64b] N. Tasneem,[64b] T. J. Gershon,[65] P. F. Harrison,[65] T. E. Latham,[65] R. Prepost,[66] and S. L. Wu[66]

(*BABAR* Collaboration)

[1]*Laboratoire d'Annecy-le-Vieux de Physique des Particules (LAPP), Université de Savoie, CNRS/IN2P3, F-74941 Annecy-Le-Vieux, France*
[2]*Universitat de Barcelona, Facultat de Fisica, Departament ECM, E-08028 Barcelona, Spain*
[3]*INFN Sezione di Bari and Dipartimento di Fisica, Università di Bari, I-70126 Bari, Italy*
[4]*University of Bergen, Institute of Physics, N-5007 Bergen, Norway*
[5]*Lawrence Berkeley National Laboratory and University of California, Berkeley, California 94720, USA*
[6]*Ruhr Universität Bochum, Institut für Experimentalphysik 1, D-44780 Bochum, Germany*
[7a]*Institute of Particle Physics, Vancouver, British Columbia, Canada V6T 1Z1*
[7b]*University of British Columbia, Vancouver, British Columbia, Canada V6T 1Z1*
[8a]*Budker Institute of Nuclear Physics SB RAS, Novosibirsk 630090, Russia*
[8b]*Novosibirsk State University, Novosibirsk 630090, Russia*
[8c]*Novosibirsk State Technical University, Novosibirsk 630092, Russia*
[9]*University of California at Irvine, Irvine, California 92697, USA*
[10]*University of California at Riverside, Riverside, California 92521, USA*
[11]*University of California at Santa Cruz, Institute for Particle Physics, Santa Cruz, California 95064, USA*
[12]*California Institute of Technology, Pasadena, California 91125, USA*
[13]*University of Cincinnati, Cincinnati, Ohio 45221, USA*
[14]*University of Colorado, Boulder, Colorado 80309, USA*
[15]*Laboratoire Leprince-Ringuet, Ecole Polytechnique, CNRS/IN2P3, F-91128 Palaiseau, France*

[16a]*INFN Sezione di Ferrara, I-44122 Ferrara, Italy*

[16b]*Dipartimento di Fisica e Scienze della Terra, Università di Ferrara, I-44122 Ferrara, Italy*

[17]*INFN Laboratori Nazionali di Frascati, I-00044 Frascati, Italy*

[18]*INFN Sezione di Genova, I-16146 Genova, Italy*

[19]*Humboldt-Universität zu Berlin, Institut für Physik, D-12489 Berlin, Germany*

[20]*Indian Institute of Technology Guwahati, Guwahati, Assam 781 039, India*

[21]*University of Iowa, Iowa City, Iowa 52242, USA*

[22]*Iowa State University, Ames, Iowa 50011, USA*

[23]*Johns Hopkins University, Baltimore, Maryland 21218, USA*

[24]*Laboratoire de l'Accélérateur Linéaire, IN2P3/CNRS et Université Paris-Sud 11,*
Centre Scientifique d'Orsay, F-91898 Orsay Cedex, France

[25]*Lawrence Livermore National Laboratory, Livermore, California 94550, USA*

[26]*University of Liverpool, Liverpool L69 7ZE, United Kingdom*

[27]*Queen Mary, University of London, London E1 4NS, United Kingdom*

[28]*University of London, Royal Holloway and Bedford New College,*
Egham, Surrey TW20 0EX, United Kingdom

[29]*University of Louisville, Louisville, Kentucky 40292, USA*

[30]*Johannes Gutenberg-Universität Mainz, Institut für Kernphysik, D-55099 Mainz, Germany*

[31]*University of Manchester, Manchester M13 9PL, United Kingdom*

[32]*University of Maryland, College Park, Maryland 20742, USA*

[33]*Massachusetts Institute of Technology, Laboratory for Nuclear Science,*
Cambridge, Massachusetts 02139, USA

[34a]*Institute of Particle Physics, Montréal, Québec, Canada H3A 2T8*

[34b]*McGill University, Montréal, Québec, Canada H3A 2T8*

[35a]*INFN Sezione di Milano, I-20133 Milano, Italy*

[35b]*Dipartimento di Fisica, Università di Milano, I-20133 Milano, Italy*

[36]*University of Mississippi, University, Mississippi 38677, USA*

[37]*Université de Montréal, Physique des Particules, Montréal, Québec, Canada H3C 3J7*

[38]*INFN Sezione di Napoli and Dipartimento di Scienze Fisiche, Università di Napoli Federico II,*
I-80126 Napoli, Italy

[39]*NIKHEF, National Institute for Nuclear Physics and High Energy Physics,*
NL-1009 DB Amsterdam, The Netherlands

[40]*University of Notre Dame, Notre Dame, Indiana 46556, USA*

[41]*Ohio State University, Columbus, Ohio 43210, USA*

[42a]*INFN Sezione di Padova, I-35131 Padova, Italy*

[42b]*Dipartimento di Fisica, Università di Padova, I-35131 Padova, Italy*

[43]*Laboratoire de Physique Nucléaire et de Hautes Energies, IN2P3/CNRS, Université Pierre et Marie*
Curie-Paris6, Université Denis Diderot-Paris7, F-75252 Paris, France

[44a]*INFN Sezione di Perugia, I-06123 Perugia, Italy*

[44b]*Dipartimento di Fisica, Università di Perugia, I-06123 Perugia, Italy*

[45a]*INFN Sezione di Pisa, I-56127 Pisa, Italy*

[45b]*Dipartimento di Fisica, Università di Pisa, I-56127 Pisa, Italy*

[45c]*Scuola Normale Superiore di Pisa, I-56127 Pisa, Italy*

[46]*Princeton University, Princeton, New Jersey 08544, USA*

[47a]*INFN Sezione di Roma, I-00185 Roma, Italy*

[47b]*Dipartimento di Fisica, Università di Roma La Sapienza, I-00185 Roma, Italy*

[48]*Universität Rostock, D-18051 Rostock, Germany*

[49]*Rutherford Appleton Laboratory, Chilton, Didcot, Oxon OX11 0QX, United Kingdom*

[50]*CEA, Irfu, SPP, Centre de Saclay, F-91191 Gif-sur-Yvette, France*

[51]*SLAC National Accelerator Laboratory, Stanford, California 94309 USA*

[52]*University of South Carolina, Columbia, South Carolina 29208, USA*

[53]*Southern Methodist University, Dallas, Texas 75275, USA*

[54]*St. Francis Xavier University, Antigonish, Nova Scotia, Canada B2G 2W5*

[55]*Stanford University, Stanford, California 94305, USA*

[56]*State University of New York, Albany, New York 12222, USA*

[57]*Tel Aviv University, School of Physics and Astronomy, Tel Aviv 69978, Israel*

[58]*University of Tennessee, Knoxville, Tennessee 37996, USA*

[59]*University of Texas at Austin, Austin, Texas 78712, USA*

[60]*University of Texas at Dallas, Richardson, Texas 75083, USA*

[61a]*INFN Sezione di Torino, I-10125 Torino, Italy*

^{61b}Dipartimento di Fisica, Università di Torino, I-10125 Torino, Italy

^{62}INFN Sezione di Trieste and Dipartimento di Fisica, Università di Trieste, I-34127 Trieste, Italy

^{63}IFIC, Universitat de Valencia-CSIC, E-46071 Valencia, Spain

^{64a}Institute of Particle Physics, Victoria, British Columbia, Canada V8W 3P6

^{64b}University of Victoria, Victoria, British Columbia, Canada V8W 3P6

^{65}Department of Physics, University of Warwick, Coventry CV4 7AL, United Kingdom

^{66}University of Wisconsin, Madison, Wisconsin 53706, USA

The decay $\tau^- \to K^- K_S \nu_\tau$ has been studied using 430×10^6 $e^+ e^- \to \tau^+ \tau^-$ events produced at a center-of-mass energy around 10.6 GeV at the PEP-II collider and studied with the *BABAR* detector. The mass spectrum of the $K^- K_S$ system has been measured and the spectral function has been obtained. The measured branching fraction $\mathcal{B}(\tau^- \to K^- K_S \nu_\tau) = (0.739 \pm 0.011(\text{stat}) \pm 0.020(\text{syst})) \times 10^{-3}$ is found to be in agreement with earlier measurements.

I. INTRODUCTION

The τ lepton provides a remarkable laboratory for studying many open questions in particle physics. With a large statistics of about 10^9 τ's produced in $e^+ e^-$ annihilation at the *BABAR* experiment, various aspects can be studied, e.g., improving the precision of spectral functions describing the mass distribution of the hadronic decays of the τ. In this work, we analyze the $\tau^- \to K^- K_S \nu_\tau$ decay[1] and measure the spectral function of this channel defined as [1]

$$V(q) = \frac{m_\tau^8}{12\pi C(q)|V_{ud}|^2} \frac{\mathcal{B}(\tau^- \to K^- K_S \nu_\tau)}{\mathcal{B}(\tau^- \to e^- \bar{\nu}_e \nu_\tau)} \frac{1}{N} \frac{dN}{dq}, \quad (1)$$

where m_τ is the τ mass [2], $q \equiv m_{K^- K_S}$ is the invariant mass of the $K^- K_S$ system, V_{ud} is an element of the Cabibbo-Kobayashi-Maskawa matrix [2], $(dN/dq)/N$ is the normalized $K^- K_S$ mass spectrum, and $C(q)$ is the phase space correction factor given by the following formula:

$$C(q) = q(m_\tau^2 - q^2)^2(m_\tau^2 + 2q^2). \quad (2)$$

According to the conserved-vector-current hypothesis [1], the $\tau^- \to K^- K_S \nu_\tau$ spectral function is related to the isovector part $(I = 1)$ of the $e^+ e^- \to K\bar{K}$ cross section:

$$\sigma^{I=1}_{e^+ e^- \to K\bar{K}}(q) = \frac{4\pi^2 \alpha^2}{q^2} V(q), \quad (3)$$

where α is the fine structure constant. The cross sections $e^+ e^- \to K^+ K^-$ and $e^+ e^- \to K_S K_L$ have been recently measured by the *BABAR* [3,4] and SND experiments [5]. Combining data from the $\tau^- \to K^- K_S \nu_\tau$ with $e^+ e^- \to K\bar{K}$ measurements, the moduli of the isovector and isoscalar form factors and the relative phase between them can obtained in a model-independent way.

The branching fraction for the $\tau^- \to K^- K_S \nu_\tau$ decay has been measured with relatively high (3%) precision by the Belle experiment [6]. The $K^- K_S$ mass spectrum was measured by the CLEO experiment [7]. In the CLEO analysis, a data set of 2.7×10^6 produced τ pairs was used, and about 100 events in the decay channel $\tau^- \to K^- K_S \nu_\tau$ were selected. In this work, using about $\sim 10^9$ τ leptons, we significantly improve upon the measurement of the spectral function for the $\tau^- \to K^- K_S \nu_\tau$ decay.

II. DATA USED IN THE ANALYSIS

We analyze a data sample corresponding to an integrated luminosity of 468 fb^{-1} recorded with the *BABAR* detector [8,9] at the SLAC PEP-II asymmetric-energy $e^+ e^-$ collider.

For simulation of $e^+ e^- \to \tau^+ \tau^-$ events the KK2f Monte Carlo generator [10] is used, which includes higher-order radiative corrections to the Born-level process. Decays of τ leptons are simulated using the Tauola package [11]. Two separate samples of simulated $e^+ e^- \to \tau^+ \tau^-$ events are used: a generic sample with τ decaying to all

---

*Present address: Wuhan University, Wuhan 430072, China.

†Present address: Università di Bologna and INFN Sezione di Bologna, I-47921 Rimini, Italy.

‡Deceased.

§Present address: University of Huddersfield, Huddersfield HD1 3DH, United Kingdom.

¶Present address: University of South Alabama, Mobile, Alabama 36688, USA.

**Also at: Università di Sassari, I-07100 Sassari, Italy.

[1]Throughout this paper, inclusion of charge-conjugated channels is implied.

significant final states, and the signal channel where $\tau^+ \to l^+ \nu_l \bar{\nu}_\tau$, $l = e$ or μ and $\tau^- \to K^- K_S \nu_\tau$. To estimate backgrounds, we use a sample of simulated generic $e^+ e^- \to \tau^+ \tau^-$ events after excluding the signal decay channel ($\tau^+ \tau^-$ background) and a sample containing all events arising from $e^+ e^- \to q\bar{q}$, $q = u, d, s, c$ and $e^+ e^- \to B\bar{B}$ processes ($q\bar{q}$ background). The $q\bar{q}$ background events with $q = u, d, s, c$ are generated using the JETSET generator [12], while $B\bar{B}$ events are simulated with EVTGEN [13]. The detector response is simulated with GEANT4 [14]. The equivalent luminosity of the simulated sample is 2-3 times higher than the integrated luminosity in data.

III. EVENT SELECTION

We select $e^+ e^- \to \tau^+ \tau^-$ events with the τ^+ decaying leptonically ($\tau^+ \to l^+ \nu_l \bar{\nu}_\tau$, $l = e$ or μ) and the τ^- decaying to $K^- K_S \nu_\tau$. Such events referred to as signal events below. The K_S candidate is detected in the $K_S \to \pi^+ \pi^-$ decay mode. The topology of events to be selected is shown in Fig. 1. Unless otherwise stated, all quantities are measured in the laboratory frame. The selected events must satisfy the following requirements:

(i) The total number of charged tracks, N_{trk}, must be four and the total charge of the event must be zero.

(ii) Among the four charged tracks there must be an identified lepton (electron or muon) and an identified kaon of opposite charge. The track origin point requirements are $|d_0| < 1.5$ cm and $|z_0| < 2.5$ cm, where $|d_0|$ and $|z_0|$ are the distances between the track and the interaction region center in transverse and longitudinal directions with respect to the beams.

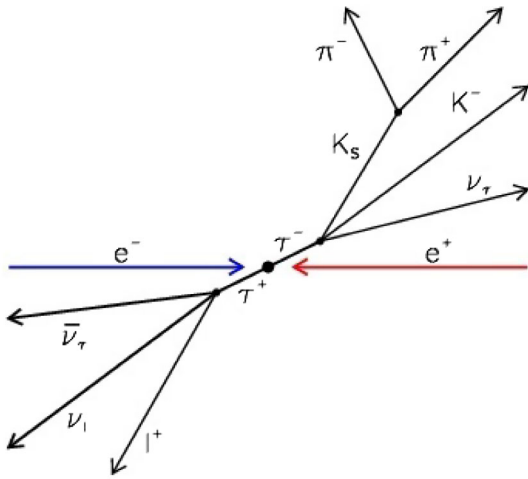(iii) To reject μ pairs and Bhabha events, the lepton candidate must have a momentum above 1.2 GeV/c, the momentum in the center-of-mass frame (c.m. momentum) must be smaller than 4.5 GeV/c, and the cosine of the lepton polar angle $|\cos \theta_l|$ must be below 0.9.

(iv) To suppress background from charged pions, the charged kaon candidate must have a momentum, p_K, above 0.4 GeV/c and below 5 GeV/c, and the cosine of its polar angle must lie between -0.7374 and 0.9005.

(v) The two remaining tracks, assumed to be pions, form the K_S candidate. The $\pi^+ \pi^-$ invariant mass must lie within 25 MeV/c^2 of the nominal K_S mass, 497.6 MeV/c^2. The K_S flight length r_{K_S}, measured as the distance between the $\pi^+ \pi^-$ vertex and the collision point, must be larger than 1 cm. The r_{K_S} distributions for data events and simulated signal events are shown in Fig. 2.

(vi) The total energy in neutral clusters, ΣE_γ, must be less than 2 GeV (Fig. 3). Here, a neutral cluster is defined as a local energy deposit in the calorimeter with energy above 20 MeV and no associated charged track.

(vii) The magnitude of the thrust [15,16] for the event, calculated using charged tracks only, must be greater than 0.875.

(viii) The angle defined by the momentum of the lepton and that of the $K^- K_S$ system in the c.m. frame must be larger than 110 degrees.

As a result of applying these selection criteria the τ background is suppressed by 3.5 orders of magnitude, and the $q\bar{q}$ background by 5.5 orders.
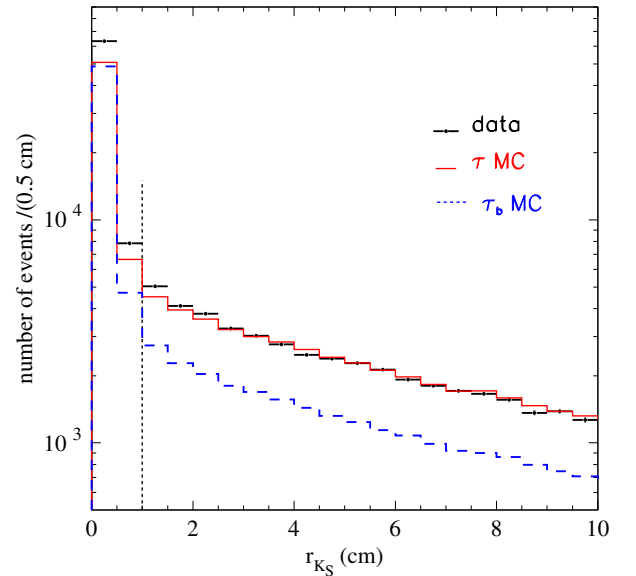

FIG. 1. Schematic view of the τ decay chains in $e^+ e^- \to \tau^+ \tau^-$ events selected for this analysis. Lepton l^+ can be electron or muon.

FIG. 2. The K_S candidates decay length distribution for data (points with errors), $\tau^+ \tau^-$ simulation events (solid histogram), and τ background simulation (dashed histogram). The vertical line indicates the boundary of the selection condition.
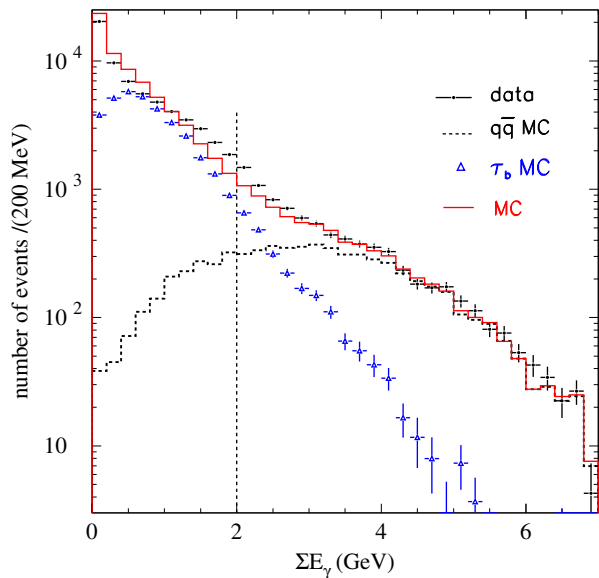
FIG. 3. Distributions of the total energy of photons in the event for data (points with errors), $\tau^+\tau^-$ and $q\bar{q}$ simulation events (solid histogram), τ background simulation (empty triangles with errors) and $q\bar{q}$ background simulation (dashed histogram). The vertical line indicates the boundary of the selection condition.

IV. DETECTION EFFICIENCY

The detection efficiency obtained after applying the selection criteria is calculated using signal Monte Carlo simulation as a function of the true $m_{K^-K_S}$ mass and is shown in Fig. 4. The efficiency is weakly dependent on $m_{K^-K_S}$. The average efficiency over the mass spectrum is about 13%. It should be noted that the K^-K_S mass
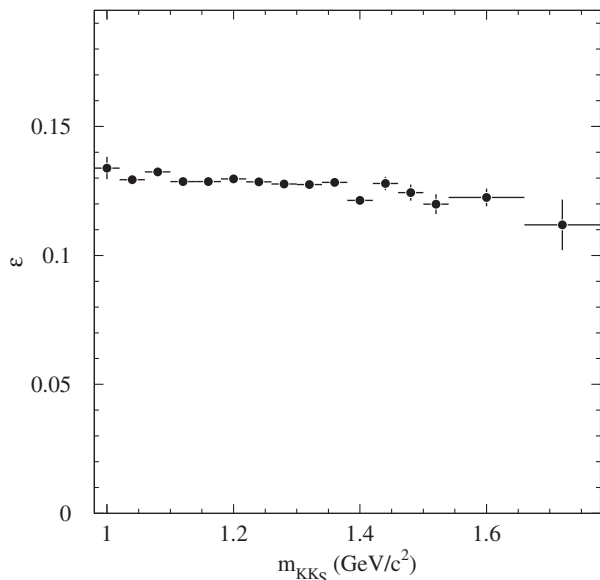

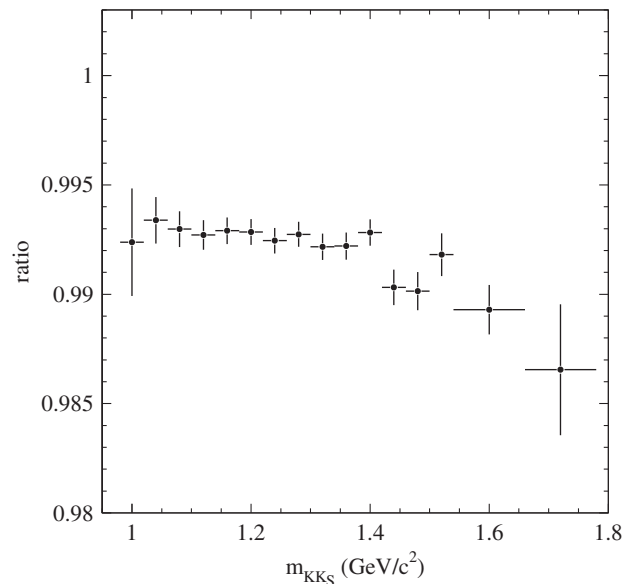FIG. 4. Selection efficiency as a function of the K^-K_S invariant mass, according to simulation.

FIG. 5. Efficiency correction factor for adjusting the simulation PID efficiency to match the efficiency measured on data, as a function of the K^-K_S mass for signal events.

resolution is about 2–3 MeV/c^2, significantly smaller than the size of the mass bin (40 MeV/c^2) used in Fig. 4. Therefore, in the following we neglect the effects of the finite K^-K_S mass resolution.

To correct for the imperfect simulation of the kaon identification requirement, the particle identification (PID) efficiences have been compared for data and simulation on high purity control samples of kaons from $D^\star \to \pi^+ D^0$, $D^0 \to K^-\pi^+$ decays [17]. We correct the simulated efficiency using the measured ratios of the efficiencies measured in data and Monte Carlo, in bins of the kaon candidate momentum and polar angle. The resulting correction factor as a function of $m_{K^-K_S}$ is shown in Fig. 5.

V. SUBTRACTION OF NON-K_S BACKGROUND

The $\pi^+\pi^-$ mass spectra for K_S candidates in data and simulated signal events are shown in Fig. 6. The data spectrum consists of a peak at the K_S mass and a flat background. To subtract the non-K_S background, the following procedure is used. The signal region is set to $\pi^+\pi^-$ masses within 0.0125 GeV/c^2 of the K_S mass (indicated by arrows in Fig. 6), and the sidebands are set to between 0.0125 and 0.0250 GeV/c^2 away from the nominal K_S mass. Let β be the fraction of events with a true K_S that fall in the sidebands, and let α be the fraction of non-K_S events that fall in the sidebands. The total number of events in the signal region plus the sidebands, N, and the number of events in the sidebands, N_{sb}, depend on the number of true K_S, N_{K_S}, and the number of non-K_S background events, N_b according to the following relation:
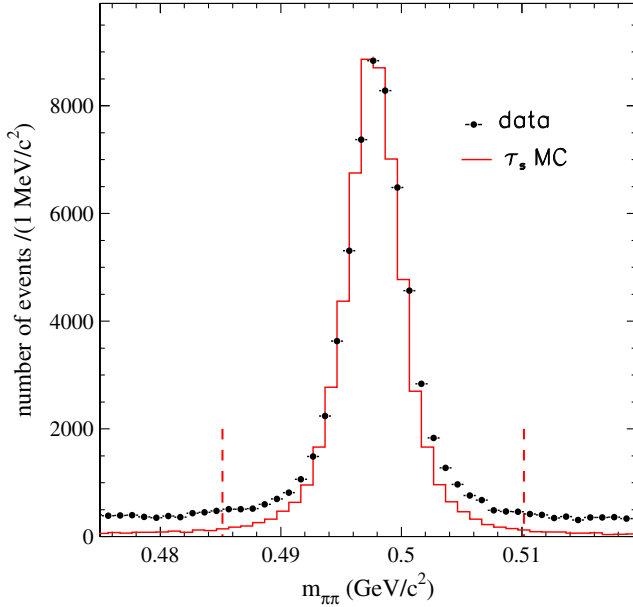
FIG. 6. The $\pi^+\pi^-$ mass spectrum for K_S candidates in data (points with errors) and signal simulation (histogram). Between the two vertical lines there is a signal region used in the procedure of non-K_S background subtraction.

$$N = N_{K_S} + N_b, \tag{4a}$$

$$N_{sb} = \alpha \cdot N_b + \beta \cdot N_{K_S} \tag{4b}$$

Therefore:

$$N_{K_S} = (\alpha N - N_{sb})/(\alpha - \beta). \tag{5}$$

The value of β is determined using τ signal simulation. It is found to be nearly independent of the $m_{K^-K_S}$ mass and is equal to 0.0315 ± 0.0015. The value of α is expected to be 0.5 for a uniformly distributed background. This is consistent with the value 0.499 ± 0.005 obtained on simulated $\tau^+\tau^-$ background events. The non-K_S background is subtracted in each $m_{K^-K_S}$ bin. Its fraction is found to be about 10% of the selected events with $m_{K^-K_S}$ near and below 1.3 GeV/c^2 and increases up to 50% above 1.6 GeV/c^2.

VI. SUBTRACTION OF τ-BACKGROUND WITH A π^0

Although the studied process $\tau^- \to K^- K_S \nu_\tau$ is not supposed to contain a π^0 in the final state, some events from background processes with a π^0 pass the selection criteria. In the following, we describe how the π^0 background contribution is subtracted.

The $K^- K_S$ mass spectra for selected data and $\tau^+\tau^-$ simulated events after subtraction of the non-K_S background are shown in Fig. 7. According to the simulation, the number
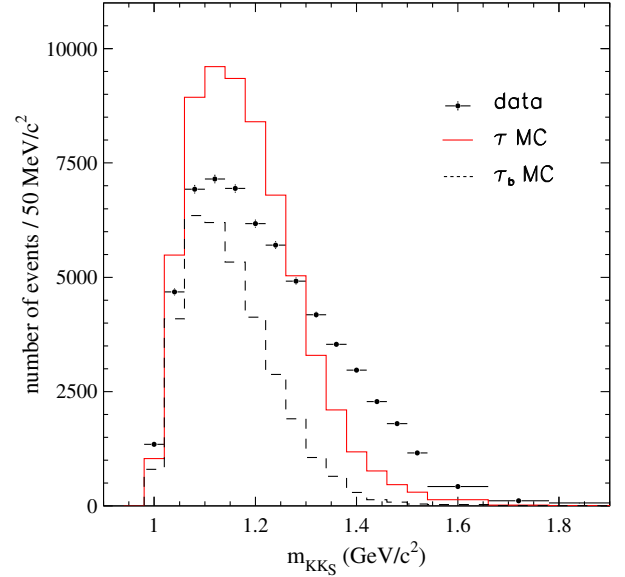

FIG. 7. The $m_{K^-K_S}$ spectra for data (points with errors), $\tau^+\tau^-$ simulation events (solid histogram), and τ background simulation (dashed histogram). The non-K_S background is subtracted.

of signal and τ-background events are of the same order of magnitude. The $\tau^+\tau^-$ background consists of events with the decay $\tau^- \to K^- K_S \pi^0 \nu_\tau$ (79%), events with a misidentified kaon from decays $\tau^- \to \pi^- K_S \nu_\tau$ (10%) and $\tau^- \to \pi^- K_S \pi^0 \nu_\tau$ (3%), and events with a misidentified lepton mainly from the decays $\tau^+ \to \pi^+ \bar{\nu}_\tau$ and $\tau^+ \to \pi^+ \pi^0 \bar{\nu}_\tau$ (7%). Thus, more than 80% of the background events contain a π^0 in the final state. It should be noted that events with a misidentified lepton have the same $m_{K^-K_S}$ distribution as signal events.

The branching fractions for the background modes without a π^0, $\tau^- \to \pi^- K_S \nu_\tau$ and $\tau^+ \to \pi^+ \bar{\nu}_\tau$, have been measured with high precision (1.7% and 0.5%) [2]. The hadronic mass spectrum for $\tau^- \to \pi^- K_S \nu_\tau$ is also well known [18] and this decay proceeds mainly via the $K^*(892)$ intermediate state. Therefore all $\tau^+\tau^-$ background without a π^0 is subtracted using Monte Carlo simulation. The amount of $q\bar{q}$ background, not shown in Fig. 7, is about 2% of selected data events. The part of this background without a π^0 is also subtracted using Monte Carlo simulation.

The branching fractions for the background modes $\tau^- \to K^- K_S \pi^0 \nu_\tau$, $\tau^- \to \pi^- K_S \pi^0 \nu_\tau$, and $\tau^+ \to \pi^+ \pi^0 \bar{\nu}_\tau$ are measured with a precision of 4.7%, 3.4%, and 0.4%, respectively. The hadronic mass spectrum is well known only for the last decay [19]. For the two other decays, only low-statistics measurements [7] are available. Therefore, we use the data to subtract the τ-background with π^0 from the $K^- K_S$ mass spectrum. To do this, the selected events are divided into two classes, without and with a π^0 candidate, which is defined as a pair of photons with an invariant mass in the range 100–160 MeV/c^2.

On the resulting sample, the numbers of signal (N_s) and background $\tau^+\tau^-$ events containing a π^0 candidate (N_b) are obtained in each $m_{K^-K_S}$ bin:

$$N_{0\pi^0} = (1 - \epsilon_s)N_s + (1 - \epsilon_b)N_b, \qquad (6a)$$

$$N_{1\pi^0} = \epsilon_s N_s + \epsilon_b N_b, \qquad (6b)$$

where $N_{0\pi^0}$ and $N_{1\pi^0}$ are the numbers of selected data events with zero and at least one π^0 candidate, and ϵ_s (ϵ_b) is the probability for signal (background) $\tau^+\tau^-$ events to be found in events with at least one π^0 candidate calculated using Monte Carlo simulation. The values ϵ_s and ϵ_b for each bin in $m_{K^-K_S}$ are measured in Monte Carlo by counting how many signal and background event candidates contain a π^0 candidate. Figure 8 shows the ϵ_s and ϵ_b measured in Monte Carlo as a function of $m_{K^-K_S}$. The efficiency ϵ_b is corrected to take into account the different π^0 efficiency between data and Monte Carlo as measured on data and simulated control samples in the ISR $e^+e^- \to \omega(783)\gamma \to \pi^+\pi^-\pi^0\gamma$ process [20]. The average correction is $\delta = 0.976 \pm 0.008$. The non-zero value of ϵ_s is due to random combinations of two spurious photons originating from beam background or nuclear interactions of charged kaons or pions. The beam-generated background is simulated by using special background events recorded during normal data-taking conditions but with a randomly generated trigger. These events are superimposed on simulated events. The following procedure is used to measure ϵ_s on data events. We compare the solution of Eqs. (6a) and (6b) described above with the solution of the same system, in which the number of events with π^0 is determined from the

fit to the two-photon invariant mass spectrum of π^0 candidates. Since the mass dependence of ϵ_s and ϵ_b is mild (Fig. 8), this comparison is performed using the full sample of selected events without splitting the sample into K^-K_S mass bins. The two-photon mass spectrum of π^0 candidates in data is shown in Fig. 9.

The spectrum in Fig. 9 is fitted by a sum of a Gaussian and a flat component. The numbers $N_{1\pi^0}$ and $N_{0\pi^0}$ on the left side of Eqs. (6a) and (6b) are substituted by $N_{1\pi^0}^\star = N_{1\pi^0} - N_{1\pi^0}^{\mathrm{lin}}$ and $N_{0\pi^0}^\star = N_{0\pi^0} + N_{1\pi^0}^{\mathrm{lin}}$, where $N_{1\pi^0}^{\mathrm{lin}}$ is the number of events under the flat component, obtained after fitting the $\gamma\gamma$ spectrum in Fig. 9. The value ϵ_b is substituted by $\epsilon_b^\star = w\epsilon_b$, where $w = 0.682 \pm 0.010$ is the fraction of events with a reconstructed π^0 for simulated $\tau^+\tau^-$ background (Fig. 9). The term "reconstructed π^0" corresponds to π^0 s in the Gaussian part in Fig. 9. The modified system of equations is

$$N_{0\pi^0}^\star = N_s + (1 - \epsilon_b^\star)N_b, \qquad (7a)$$

$$N_{1\pi^0}^\star = \epsilon_b^\star N_b. \qquad (7b)$$

In Eqs. (7a) and (7b) the top line contains all events without a reconstructed π^0, while the lower line contains events with at least one reconstructed π^0. After subtracting the spurious π^0s corresponding to the flat background in Fig. 9, Eqs. (7a) and (7b) no longer contains ϵ_s nor a contribution from the π^0 background.

The average value of ϵ_b from Fig. 8 is 0.720 ± 0.003, giving $\epsilon_b^\star = 0.491 \pm 0.008$ on the average. This value is then corrected by the reconstructed π^0 efficiency correction
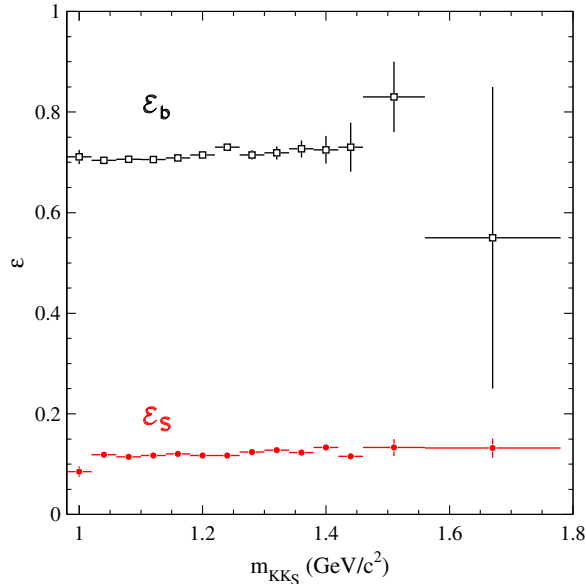

FIG. 8. The probabilities ϵ_s and ϵ_b used in Eqs. (6a) and (6b) as functions of the K^-K_S mass, measured on simulated events.
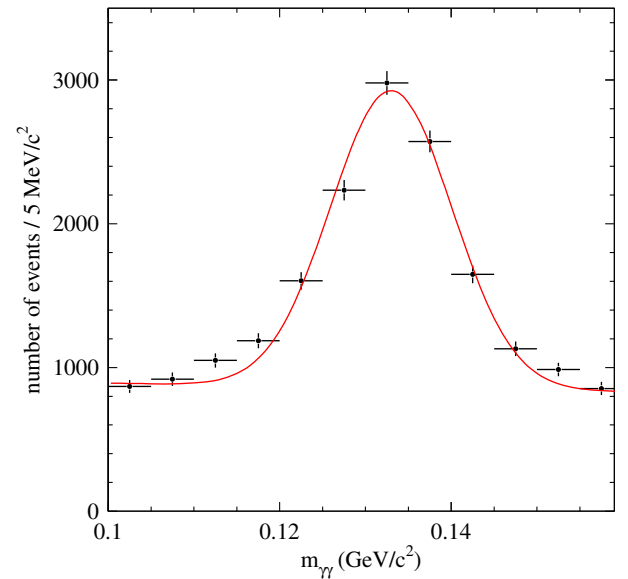

FIG. 9. Two-photon invariant mass spectrum of π^0 candidates in data. The curve corresponds to the fit function, described in text.
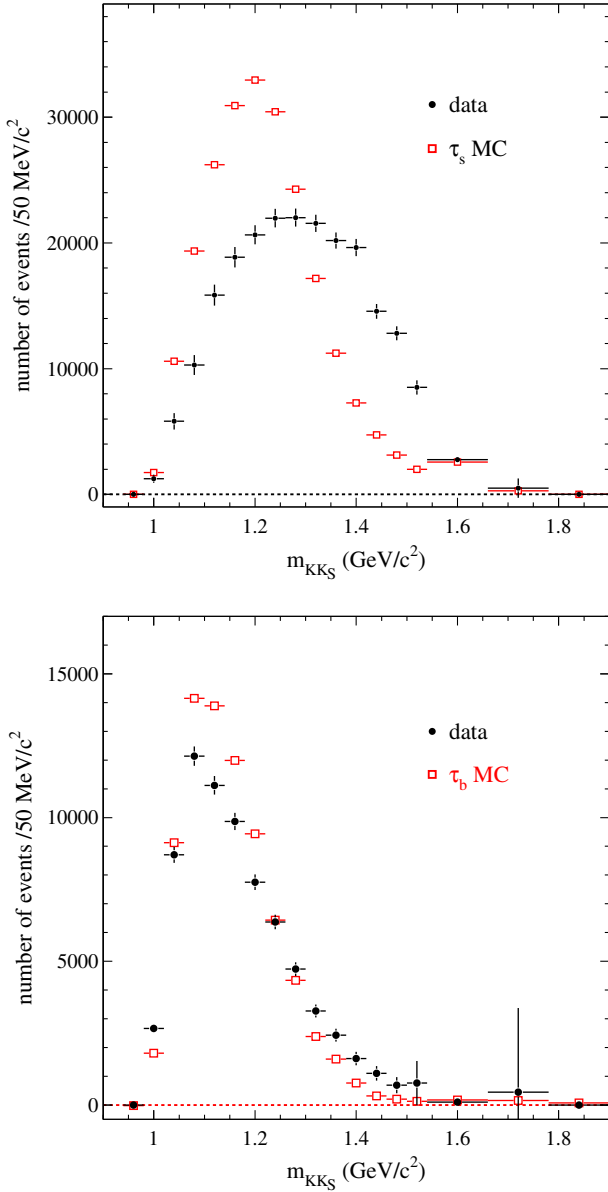
FIG. 10. Measured $m_{K^- K_S}$ spectra for signal events (top) and τ background events with π^0 (bottom) in comparison with the τ signal (τ_S) and τ background (τ_b) Monte Carlo simulation.

factor δ, as discussed above. The number of signal events, N_s, obtained by solving Eqs. (7a) and (7b) and using the corrected value of $\epsilon_b^\star$ is about 1% higher than the previous one, derived from Eqs. (6a) and (6b). This 1% shift in N_s is explained by the difference between data and Monte Carlo simulation in ϵ_s.

To obtain the final $K^- K_S$ mass spectrum we return to Eqs. (6a) and (6b). Based on the above study of the π^0 systematics we must correct the efficiencies ϵ_s and ϵ_b. First, we correct the value of ϵ_b by the π^0 efficiency correction $1 - w(1 - \delta) \simeq 0.984 \pm 0.006$, where w and δ are defined above. Then we adjust the value of ϵ_s by a factor 1.05 ± 0.05 to take into account the above-mentioned 1%

correction in flat background simulation. Then the number of simulated $\tau^+ \tau^-$ background events without a π^0 is multiplied by a factor of $p = 0.92 \pm 0.02$ to take into account the difference between experimental τ branching fractions and branching fractions used in the Tauola Monte Carlo generator. With these corrected values for ϵ_s and ϵ_b we solve Eqs. (6a) and (6b) for each $K^- K_S$ mass bin and obtain mass spectra for signal (N_s) and background (N_b).

The efficiency corrected signal mass spectrum, using the signal efficiency from Fig. 4, is shown in Fig. 10 (top), in comparison with the simulation. The τ-pair $m_{K^- K_S}$ background spectrum [Fig. 10 (bottom)] is compared with simulation without efficiency correction. Spectra are normalized to the same number of events. We find a substantial difference between data and simulation for the signal spectrum, and better agreement for the background spectrum.

VII. SYSTEMATIC UNCERTAINTIES

This section lists all the uncertainties in the parameters used in this analysis, and estimates the overall systematic uncertainty on the $\tau^- \to K^- K_S \nu_\tau$ branching fraction and the $K^- K_S$ mass spectrum.

The subtraction of non-K_S background is described in Sec. V. To check the procedure of the non-K_S background subtraction, we varied the coefficients of α and β within their uncertainties, which leads to a systematic uncertainty of 0.4% in the $\tau^- \to K^- K_S \nu_\tau$ branching fraction. This uncertainty is independent of the $K^- K_S$ mass.

The PID corrections were discussed in Sec. IV. The systematic uncertainty due to data-Monte Carlo simulation difference in particle identification is taken to be 0.5%, independent of the $K^- K_S$ mass. The uncertainty on how well the Monte Carlo simulates the tracking efficiency is estimated to be 1%.

Figure 11 shows the $m_{K^- K_S}$ spectra for selected data events with and without a π^0 candidate near the endpoint $m_{K^- K_S} = m_\tau$ compared to simulated $q\bar{q}$ events. It appears that the number of data and simulated $q\bar{q}$ events are in reasonable agreement at $m_{K^- K_S} > m_\tau$, where all data events are expected to be from the $q\bar{q}$ background. We take the observed difference between data and Monte Carlo near the end point $M_{K^- K_S} = m_\tau$ in Fig. 11 as an uncertainty on the $q\bar{q}$ background. This leads to an uncertainty on $\mathcal{B}(\tau^- \to K^- K_S \nu_\tau)$ of 0.5%.

The uncertainty associated with the subtraction of the $\tau^+ \tau^-$ background with π^0's is estimated by varying the efficiencies ϵ_s and ϵ_b used in Eqs. (6a) and (6b) within their systematic uncertainties: 5% in ϵ_s (uncertainty in the number of spurious π^0s) and 6% in ϵ_b (uncertainty in numbers of both spurious and reconstructed π^0s). The corresponding contribution to the systematic uncertainty on $\mathcal{B}(\tau^- \to K^- K_S \nu_\tau)$ is 2.3%. For the $m_{K^- K_S}$ spectrum this
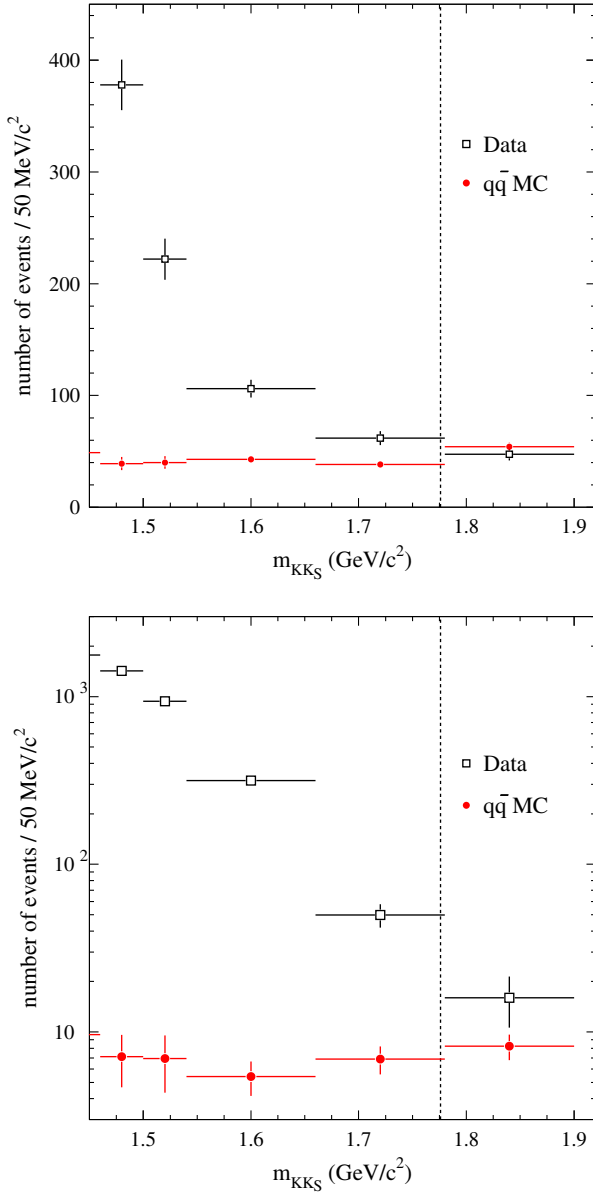
FIG. 11. $K^- K_S$ mass spectra near the end point $M_{K^- K_S} = m_\tau$ for selected data and $q\bar{q}$ simulated events without (top) and with (bottom) a π^0 candidate. The vertical line indicates the τ mass.

TABLE I. The systematic uncertainties on $B(\tau^- \to K^- K_S \nu_\tau)$ from different sources.

Sources	Uncertainty (%)
Luminosity	0.5
Tracking efficiency	1.0
PID	0.5
Non-K_S background subtraction	0.4
$\tau^+ \tau^-$ background without π^0	0.3
$\tau^+ \tau^-$ background with π^0	2.3
$q\bar{q}$ background	0.5
Total	2.7

TABLE II. Measured spectral function (V) of the $\tau^- \to K^- K_S \nu_\tau$ decay, in bins of $m_{K^- K_S}$. The columns report: the range of the bins, the normalized number of events, the value of the spectral function. The first error is statistical, the second systematic.

$m_{K^- K_S}$ (GeV/c^2)	$N_s/N_{\text{tot}} \times 10^3$	$V \times 10^3$
0.98–1.02	5.6 ± 1.4	$0.071 \pm 0.018 \pm 0.006$
1.02–1.06	26.0 ± 2.7	$0.331 \pm 0.034 \pm 0.026$
1.06–1.10	46.0 ± 3.2	$0.593 \pm 0.042 \pm 0.042$
1.10–1.14	70.8 ± 3.5	$0.934 \pm 0.046 \pm 0.056$
1.14–1.18	84.4 ± 3.4	$1.148 \pm 0.047 \pm 0.057$
1.18–1.22	92.3 ± 3.3	$1.309 \pm 0.046 \pm 0.052$
1.22–1.26	98.2 ± 3.2	$1.468 \pm 0.048 \pm 0.044$
1.26–1.30	98.4 ± 3.2	$1.569 \pm 0.050 \pm 0.042$
1.30–1.34	96.3 ± 3.0	$1.663 \pm 0.052 \pm 0.042$
1.34–1.38	90.2 ± 2.9	$1.715 \pm 0.052 \pm 0.039$
1.38–1.42	87.8 ± 3.1	$1.873 \pm 0.066 \pm 0.039$
1.42–1.46	65.1 ± 2.6	$1.597 \pm 0.064 \pm 0.032$
1.46–1.50	57.3 ± 2.5	$1.666 \pm 0.073 \pm 0.032$
1.50–1.54	38.1 ± 2.5	$1.361 \pm 0.090 \pm 0.023$
1.54–1.66	36.9 ± 2.4	$0.785 \pm 0.049 \pm 0.013$
1.66–1.78	6.6 ± 10.2	$0.986 \pm 1.520 \pm 0.014$

uncertainty varies from 9% at $m_{K^- K_S} < 1.1$ GeV/c^2 to 1% at 1.7 GeV/c^2.

The 2% uncertainty in the correction factor p (Sec. VI), associated with τ branching fractions without a π^0, leads to the 0.3% uncertainty in the branching ratio. The mass-dependent uncertainty is 2% at $K^- K_S$ mass below 1.1 GeV and 0.1% for 1.7 GeV/c^2.

The systematic uncertainties from different sources, shown in Table I, are combined in quadrature. The total systematic uncertainty for the branching fraction $\mathcal{B}(\tau^- \to K^- K_S \nu_\tau)$ is 2.7%. The systematic uncertainties for the mass spectrum are listed in Table II. They gradually decrease from $\simeq$9% at $m_{K^- K_S} = 1$ GeV/c^2 to 1.5% at

$m_{K^- K_S} = m_\tau$. Near the maximum of the mass spectrum (1.3 GeV/c^2) the uncertainty is about 2.5%.

VIII. THE RESULTS

The branching ratio of the $\tau^- \to K^- K_S \nu_\tau$ decay is obtained using the following expression:

$$\mathcal{B}(\tau^- \to K^- K_S \nu_\tau) = \frac{N_{\text{exp}}}{2 L B_{\text{lep}} \sigma_{\tau\tau}}$$

$$= (0.739 \pm 0.011 \pm 0.020) \times 10^{-3}, \quad (8)$$

where $N_{\text{exp}} = 223741 \pm 3461$ (error is statistical) is the total number of signal events in the spectrum in Fig. 12, $L = 468.0 \pm 2.5$ fb^{-1} is the *BABAR* integrated luminosity [21], $\sigma_{\tau\tau} = 0.919 \pm 0.003$ nb is the $e^+ e^- \to \tau^+ \tau^-$ cross section at 10.58 GeV [10] and $B_{\text{lep}} = 0.3521 \pm 0.0006$ is
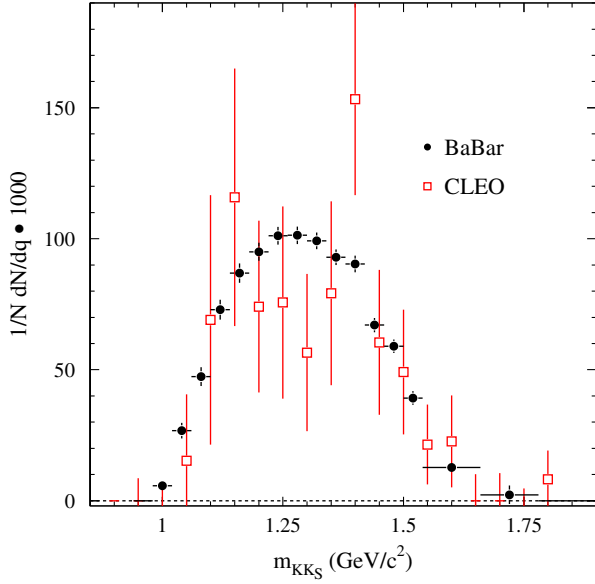
FIG. 12.   Normalized $K^- K_S$ invariant mass spectrum for the $\tau^- \to K^- K_S \nu_\tau$ decay measured in this work (filled circles) compared to the CLEO measurement [7] (empty squares). Only statistical uncertainties are shown.
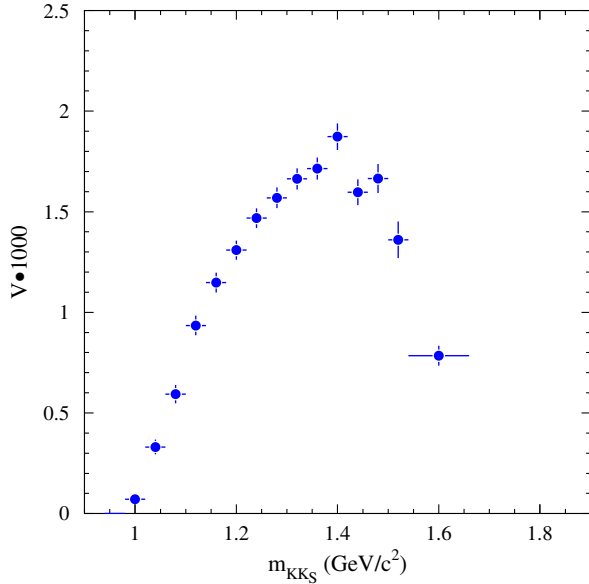

FIG. 13.   Measured spectral function for the $\tau^- \to K^- K_S \nu_\tau$ decay. Only statistical uncertainties are shown.

the world average sum of electronic and muonic branching fractions of the τ lepton [2]. The first uncertainty in (8) is the statistical, the second is systematic. Our result agrees

well with the Particle Data Group (PDG) value $(0.740 \pm 0.025) \times 10^{-3}$ [2], which is determined mainly by the recent Belle measurement $(0.740 \pm 0.007 \pm 0.027) \times 10^{-3}$ [6].

The measured mass spectrum $m_{K^- K_S}$ for the $\tau^- \to K^- K_S \nu_\tau$ decay is shown in Fig. 12 and listed in Table II. Our $m_{K^- K_S}$ spectrum is compared with the CLEO measurement [7]. The *BABAR* and CLEO spectra are in good agreement. The spectral function $V(q)$ calculated using Eq. (1) is shown in Fig. 13 and listed in Table II. Due to the large error in the mass interval 1.66–1.78 GeV/c^2, which exceeds the scale of Fig. 13, the value of $V(q)$ in this interval is not shown in Fig. 13.

IX. CONCLUSIONS

The $K^- K_S$ mass spectrum and vector spectral function in the $\tau^- \to K^- K_S \nu_\tau$ decay have been measured by the *BABAR* experiment. The measured $K^- K_S$ mass spectrum is far more precise than CLEO measurement [7] and the branching fraction $(0.739 \pm 0.011 \pm 0.020) \times 10^{-3}$ is comparable to Belle's measurement [6].

[1] Y. S. Tsai, Phys. Rev. D **4**, 2821 (1971); **13**, 771(E) (1976).

[2] C. Patrignani *et al.* (Particle Data Group), Chin. Phys. C **40**, 100001 (2016) and 2017 update.

[3] J. P. Lees *et al.* (*BABAR* Collaboration), Phys. Rev. D **88**, 032013 (2013).

[4] J. P. Lees *et al.* (*BABAR* Collaboration), Phys. Rev. D **89**, 092002 (2014).

[5] M. N. Achasov *et al.* (SND Collaboration), Phys. Rev. D **94**, 112006 (2016).

[6] S. Ryu *et al.* (Belle Collaboration), Phys. Rev. D **89**, 072009 (2014).

[7] T. E. Coan *et al.* (CLEO Collaboration), Phys. Rev. D **53**, 6037 (1996).

[8] B. Aubert *et al.* (*BABAR* Collaboration), Nucl. Instrum. Methods Phys. Res., Sect. A **479**, 1 (2002).

[9] B. Aubert *et al.* (*BABAR* Collaboration), Nucl. Instrum. Methods Phys. Res., Sect. A **729**, 615 (2013).

[10] S. Jadach, B. F. Ward, and Z. Was, Comput. Phys. Commun. **130**, 260 (2000).

[11] S. Jadach, Z. Wąs, R. Decker, and J. H. Kühn, Comput. Phys. Commun. **76**, 361 (1993).

[12] T. Sjöstrand, S. Mrenna, and P. Skands, J. High Energy Phys. 05 (2006) 026.

[13] D. J. Lange, Nucl. Instrum. Methods Phys. Res., Sect. A **462**, 152 (2001).

[14] S. Agostinelli *et al.* Nucl. Instrum. Methods Phys. Res., Sect. A **506**, 250 (2003).

[15] E. Farhi, Phys. Rev. Lett. **39**, 1587 (1977).

[16] S. Brandt, C. Peyrou, R. Sosnowski, and A. Wroblewski, Phys. Lett. **12**, 57 (1964).

[17] D. Boutigny *et al.* (*BABAR* Collaboration), SLAC Report No. SLAC-R-0504, 2010.

[18] D. Epifanov *et al.* (Belle Collaboration), Phys. Lett. B **654**, 65 (2007).

[19] M. Fujikawa *et al.* (Belle Collaboration), Phys. Rev. D **78**, 072006 (2008).

[20] B. Aubert *et al.* (*BABAR* Collaboration), Phys. Rev. D **70**, 072004 (2004).

[21] J. P. Lees *et al.* (*BABAR* Collaboration), Nucl. Instrum. Methods Phys. Res., Sect. A **726**, 203 (2013).